

## Simultaneous hydroforming of bulge- and T-zone in 70/30 brass and 304 stainless steel tubes

A. Ashofteh\* , M. Mosavi Mashhadi and S. Seifollahpour  
School of Mechanical Engineering, College of Engineering, University of Tehran, Tehran, Iran

### ARTICLE INFO

#### Article history:

Received: 1 December 2018

Accepted: 9 May 2019

#### Keywords:

Tube Hydroforming

FE simulation

pressure path

bulge zone

T-way

### ABSTRACT

Hydroforming process is largely used for the production of tubular parts in various industries, and has advantages such as less weight, higher quality, more strength and fewer production cost compared to the conventional methods of production. The aim of this study is forming a tube-shaped part with a special geometry that has both bulge- and T-zones with tube hydroforming process. The forming operations were performed on 304 stainless steel and 70/30 brass tubes, and a finite element (FE) model was used to achieve the best forming conditions. To validate FE model, firstly, several experimental tests were performed with different process parameters, and then the results were compared with the FE model in terms of the formed profile and the distribution of thickness. After validation of FE model, various pressure paths were studied and the best one between them was chosen. Finally, the part was formed correctly by the selected pressure path without defects like wrinkling or tearing, and the desired geometry was fully filled.

### 1. Introduction

The needs for the structures with high strength and low weight cause to use light and robust alloys and new manufacturing method which one of them is Hydroforming (HF). Advantages of HF contain the possibility of decreasing the production steps, increasing the strength to weight ratio, increasing dimension accuracy and tightening the tolerances [1, 2].

Hydroforming process divided into two main branches: sheet hydroforming (SHF), which produce planer metal part with complicated shape, and tube hydroforming (THF), which use for production tubular components. In SHF process, sheet is formed in the cavity with pressure of fluid and actually is stamping process with a soft punch (fluid). Some advantage of SHF is deeper drawing ratio, higher quality of final product and smoother thickness distribution. In THF process, the raw material is tube and depending on the shape of the mold cavities whole or parts of the tube perimeter were formed. Usually in THF process divided into two types [3-7]:

- 1- Forming that occur in whole section simultaneously, like changing the tube section from

the circle to square or polygon and producing stepped tube.

- 2- Forming that occur in a portion of the tube, like producing X-shape and Y-shape joints.

The main challenge in THF process is the production of parts without any defects like tearing, severe thinning and wrinkling. Affecting parameters in THF process contain the dimension of the primary tube (diameter, thickness, length, etc.) and genre of the tube (properties, formability, cost, etc.). Axial displacement and fluid pressure have the most important role in the defects controlling [4].

In many studies, the finite-element (FE) model which validated with the experimental results was used to find optimal pressure and axial feed, and it has been shown that the best pressure path for various tube geometries and sizes is different [2]. One of the advantages of using the FE model is identifying areas that are susceptible to damage, such as corners, where thinning or wrinkling may occur, and then take preventive actions in these areas [8, 9]. Different methods such as genetic algorithm [10], fuzzy logic [11], multi-objective optimization [12, 13], etc. have been used to

\* Corresponding author. Tel.: +98-910-807-0521; e-mail: [a.ashofteh@ut.ac.ir](mailto:a.ashofteh@ut.ac.ir); Fax: +98-21-82096799

optimize the pressure path. In all of these methods, attempts are made to optimize the procedure of the operation. Typically, several factors, such as minimum wall thickness, perfect formation of corners and lack of defects, are used as criteria for selecting optimal conditions [5, 7, 14, 15]. Previous researches have investigated the effect of various factors such as geometry, material, coefficient of friction, strain hardening and anisotropy on the complete formation and the distribution of the final thickness [16-22]. In this study, production of an asymmetric and combinatorial geometry of T-way and bulging with THF was studied. The shape of the part creates some limitation in process parameters, and therefore, material flow controlling in the middle sections of the tube was very complicated. A simple and approximate but high-precision method, based on the finite-element simulation, was used to find the appropriate pressure path, and the results after the production of the part with the selected path showed that this method is accurate enough.

## 2. Materials and methods

### Process introduction

The target piece of this study was a combination of bulged, and T-shape tube and Figure 1 show its view and dimensions. Special geometry and limitation of material flow in middle section of the tube were caused that proper choosing of the pressure path be critical for complete forming and appropriate thickness distribution in two portions.

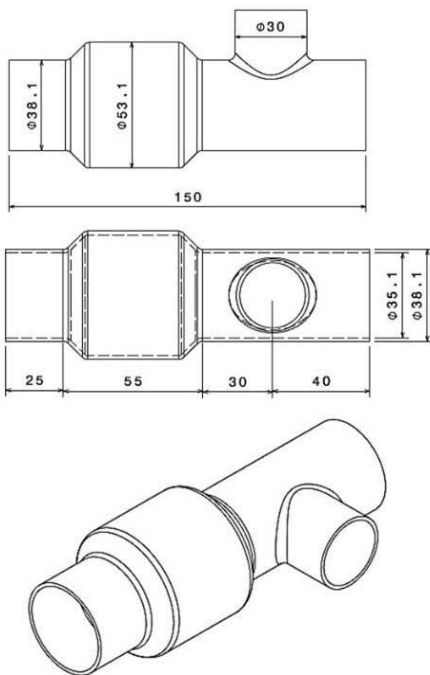


Figure 1. views of the target tube after forming process with its dimensions (all numbers are in millimeters).

The forming process was included two steps: calibration and forming. In calibration step, after inserting the tube in the mold and sealing operation, fluid entered and its pressure

increased. This step was done without any axial displacement. In forming step, the pressure was increased and axial feeding applied, simultaneously. Accurate formation of T-zone (TZ) needs counter punch but in this case for limited material flow, it was no needs to movable counter punch and so, it was fixed. Figure 2 shows a schematic pressure path.

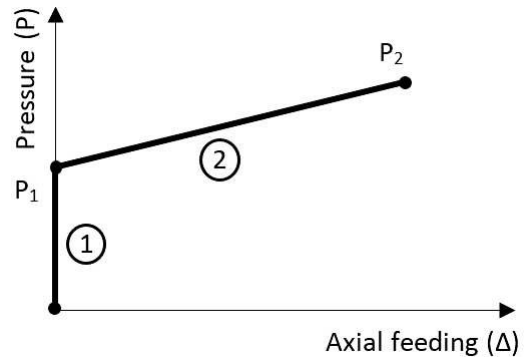


Figure 2. schematic pressure path, step 1(calibration): increasing internal pressure without axial feeding, step 2 (forming): increasing internal pressure with axial feeding simultaneously; ( $P_1$ : first step pressure,  $\Delta$ : displacement of punches,  $P_2$ : maximum pressure).

The calibration pressure was applied to prevent stretching in the bulge zone (BZ) during the forming stage, and its amount ( $P_1$ ) was obtained from FE simulation. The TZ had a smaller area than BZ and hence, higher pressure was needed. Forming pressure ( $P_2$ ) was calculated through an approximate simulation-based approach, which is described below.

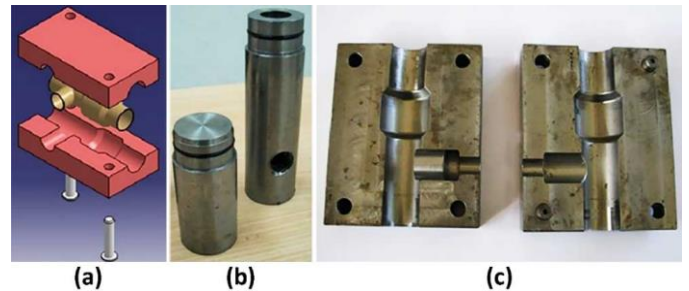


Figure 3. (a) CAD view of formed tube and molds, (b) axial punches and (c) manufactured molds.

### Tube materials

The ways to compensate material flow constraints in the middle section of the tube were increasing the pressure and axial loads. Increasing the pressure may cause severe thinning or tearing the tube; hence, complete formation of this piece may be impossible on some materials; therefore, the forming operation was done on ASTM SS304 (1.5 mm thickness) and 70/30 brass (1 mm thickness) tubes, which had high formability. The chemical compositions of tubes are shown in

Table 1.

**Table 1.** chemical composition of stainless steel (SS304) and 70/30 brass tubes [23, 24].

SS304	element	Cr	Ni	C	P	S	Si	Fe
	percentage	18.8	8.3	0.07	0.035	0.027	0.63	Base element
70/30 brass	element	Cu	Zn	Fe	Sb			
	percentage	69.8	30.095	0.048	0.057			

Annealing was performed on tubes to increase the formability. This process was done for steel tubes by holding them for 90 minutes at 950 °C, and then cooling them in the air. Brass tubes were kept at a temperature of 530 °C for 90 minutes and then cooled in the furnace. Argon vacuum furnace was used for brass tubes annealing.

**2.3 Mold and its component**

Mold containing two stationary plates that fix together with bolts. After fixing mold, sealing was performed for axial and counter punches with O-rings. CAD view of formed tube and molds, axial punches and manufactured molds are shown in Figure 3.

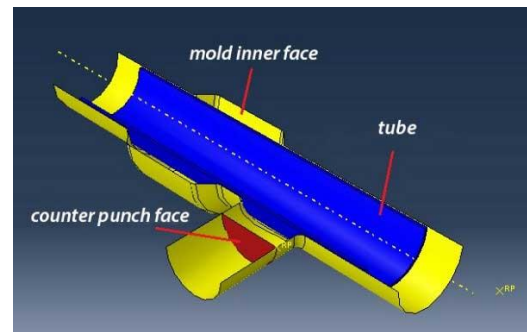


**Figure 4.** CAD model of tube and mold in ABAQUS software.

**2.4 FE simulation**

Finite-element modeling and simulating process were carried out by ABAQUS commercial software and because of symmetry about one plane, half of mold, tube and punches were modeled that seen in Figure 4. Axial movement of punches was considered with edge displacement of the tube ends which will be described in the boundary condition.

Model type for mold and tube was considered rigid and deformable, respectively; and mold was modeled as a shell to reduce the run time. Length and diameter of the tube were modeled in real size (165 mm and 38.1 mm). A reference point was assigned to mold and counter punch for boundary conditions definition. Mechanical properties of the tubes such as density, elastic and plastic parameters, was applied according to

Table 2. Model was supposed isotropic and so it obeys from  $\sigma = \sigma_y + K\varepsilon^n$  equation.

**Table 2.** mechanical properties of SS304 and 70/30 brass [23, 24].

	$\rho$ (Kg/cm <sup>3</sup> )	E (GPa)	$\nu$	$\sigma_y$ (MPa)	n	K (MPa)
SS304	7900	196	0.3	205	0.688	1400
70/30 brass	8550	150	0.375	130	0.49	895

Dynamic explicit analysis was selected for this process that is suitable for a large amount of strain. Since forming process was done in room temperature, so tube was not sensitive to strain rate, therefore, for reducing analysis time, time was considered 0.0015. Finally, stress, plastic strain, displacement and pressure were selected as the outputs.

Mechanical contact with tangential behavior and penalty expression was set as the contact condition, and according to previous simulation in HF lab, friction coefficient was set 0.14.

Fix and symmetry constraints were applied to the mold and edge of the tube, respectively. Axial feeding was performed

by creating a motion on the edges of the tube, and the control of these movements was carried out with the maximum

displacement and amplitude management, which applied to each end, separately.

Since the tube was solid, C3D8R (8 nodes 3D element) from the explicit library was used to mesh it. Mold and counter punch surface were meshed with R3D4 (4 nodes discrete rigid elements) elements. The longitudinal and thickness mesh size of the tube was considered to be 0.001 and 0.0006 mm, respectively. In addition, mold and counter punch mesh size were considered 0.0015 mm. Simulation and running the model, with various mesh sizes, was shown that these sizes

are appropriate, and the smaller mesh sizes only increase the running time.

**3. Model validation**

In the modeling process, a few tests were carried out under different conditions, and then the FE model was run under experimental conditions. Comparison of real and simulation results with each other showed that empirical results confirm the model's behavior. After the model validation, important parameters like maximum pressure, pressure path, axial feeding and their effects on thickness distribution and tube complete forming (wrinkling or not wrinkling) were investigated with simulation.

Table 3 values, to verify the simulation results; then, the model was run with the same parameters. Figure 5 shows simulation and experimental results for three cases.

At the time of forming process, firstly, the pressure of the fluid was increased to 22 MPa (P1), without applying the axial feeding, and the calibration was done; then the punches

**Table 3.** axial feeding values for No.1 and 2 punches in three experimental tests on SS304.

Test No.	LAF	RAF
#1	10mm	3mm
#2	1mm	13mm
#3	14mm	5mm

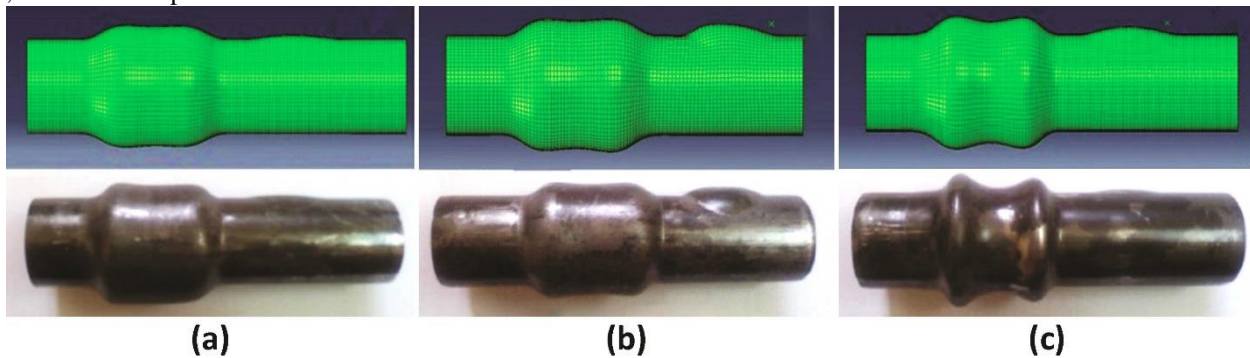
According to Figure 5, the simulation and experimental results were very close to each other and the values of the T height, diameter and profile of the BZ were also confirmed

**3.1 SS304 tube**

As mentioned earlier, the determinant parameters in the tube forming process in this study were calibration pressure (P<sub>1</sub>), maximum pressure (P<sub>2</sub>), left punch axial feeding (LAF) and right punch axial feeding (RAF). The pressure P<sub>1</sub> was applied in beginning of the process for the calibration operation and to create complete contact between tube and mold. In order to prevent the wrinkling, value of P<sub>1</sub> should be such that, the tube yielded in BZ at the beginning of the punch displacement. After performing several simulations, it was founded that the pressure of 22 MPa is suitable for the calibration of the SS304 tubes.

Empirical tests were shown that the tubes, at a pressure of approx. 36 MPa, were torn from the weld seam; therefore, the P<sub>2</sub> was considered to be the equivalent value. Three tests were performed according to started moving simultaneously, while the pressure was increased. The results were shown that in #1 and #2, when the pressure reached to 36 MPa, the tubes were torn from the weld seam, but BZ formed almost completely and no traces of wrinkling were observed in the tubes. Higher axial feeding was caused wrinkling in #3 in BZ.

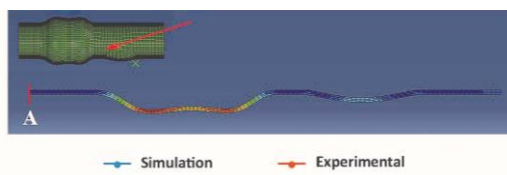
this; therefore, these similarities were the reason for the reliability of the model.



**Figure 5.** comparison between simulated formed profile and experimental results (a) test #1, (b) test #2 and (c) test #3.

The thickness distribution in the simulated model and the formed tubes were compared to each other, and results are shown in Figure 6. These results confirmed that the model accurately predicts the actual behavior of the tubes. As shown in Figure 6, the value of the thickness and its

distribution in the BZ in experimental and simulation results were close to each other, but in the TZ, a little more difference was observed; generally, the greatest difference between simulation and experimental results, in the worst case, was below 7%.



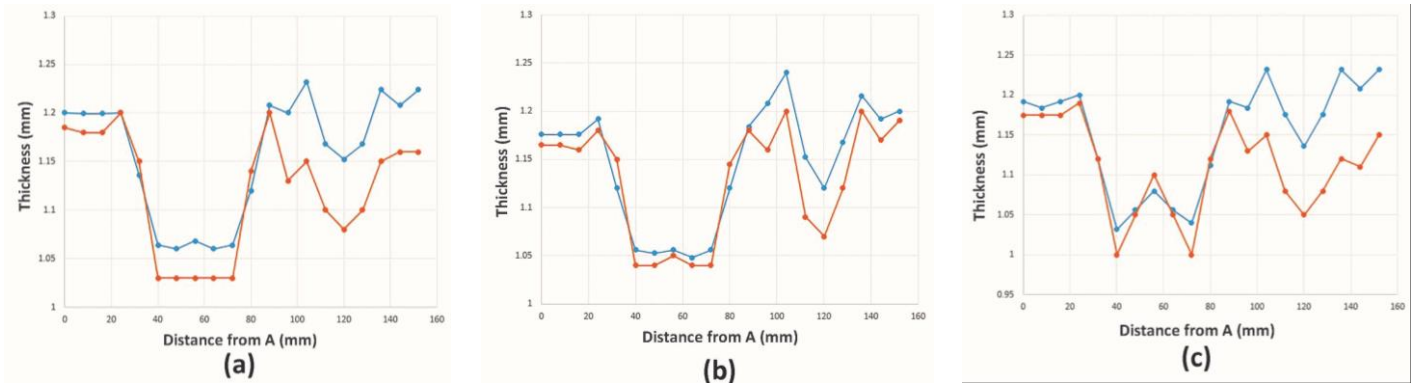


Figure 6. comparison between simulated thickness distribution and experimental results; (a) test #1, (b) test #2 and (c) test #3.

### 3.2 70/30 brass tube

Brass has a lower yield strength than steel, and hence needs less calibration and maximum pressures in forming process. According to the steel tube procedure, performing several

mentioned pressures; their specifications are shown in Table 4 and the formed tube and the simulated model can be seen in Figure 7.

**Table 4.** axial feeding values for No.1 and 2 punches in two experimental tests on the brass tube.

TEST NO.	LAF	RAF
#1	3.5mm	0mm
#2	25mm	1mm

sample tests was shown that the values of 10 MPa and 14.5 MPa are suitable for calibration and maximum pressure, respectively. For simulation validation, two samples were formed with different axial feeds and based on the above-

A quick comparison of the formed tubes and the simulated models indicates the behavioral conformance of the model, and for example; one evidence is the bottom right corner of the BZ in Figure 7-b, which was created due to exorbitance axial feeding and can be seen in both images. The comparison of the thickness distribution in the model and the tube is shown in **Error! Reference source not found.**, and the existence of a maximum difference of 5% indicates validation of the model.

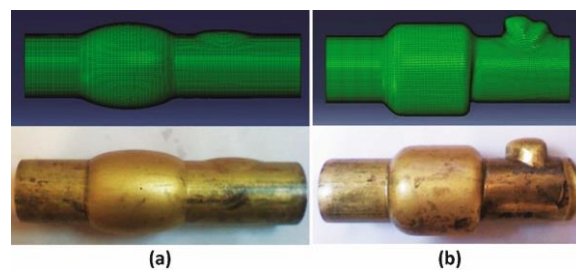
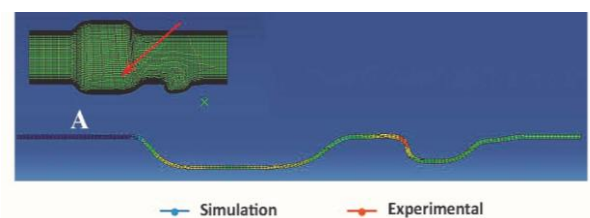


Figure 7. comparison between simulated foamed profile and experimental results (a) test #1, (b) test #2.



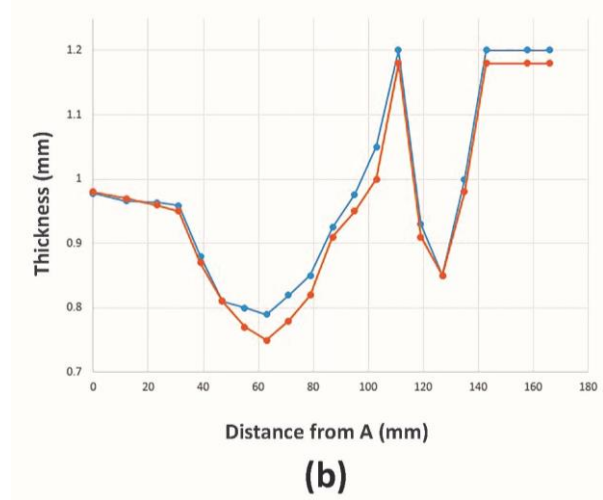
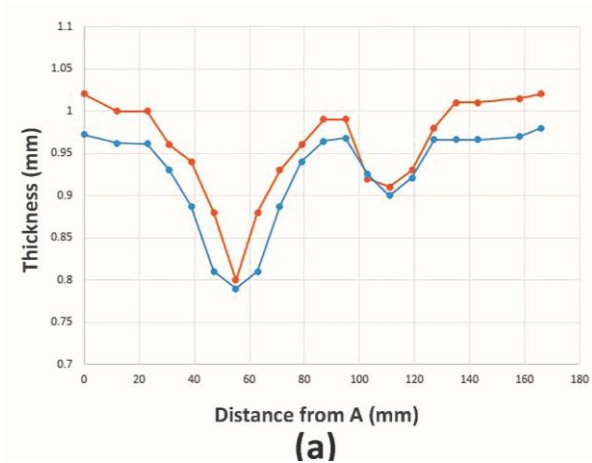


Figure 8. comparison between simulated thickness distribution and experimental results, (a) test #1, (b) test #2.

#### 4. Results and discussion

The validated model based on experimental tests, which was described in the previous section was the basis for finding the optimal pressure path for the forming process; therefore, different paths, based on full factorial design of experiments (DoE), were investigated and the best path was selected for each material.

##### 4.1 SS304 tube

The maximum pressure before tearing for the steel tube, in bulge test without applying the axial feeding was 36 MPa, but since the presence of the axial feeding caused delaying tube rapture, the forming processes were investigated for three pressures of 36, 40 and 45 MPa. Criterion of the best pressure path primarily was non-wrinkling and after that

complete filling of mold corners. Value of the LAF and RAF for SS304 tubes was 4, 6, 8 and 10 mm and 10, 13, 16 and 19 mm, respectively. Asymmetry in the shape of the mold caused the difference in the axial feeds in both sides of the tube. The reason for the lesser LAF than the RAF was the lower need for material flow in the BZ than to the TZ. In other words, the forming of the tubes was investigated at three different pressure levels, that each level had two distinct pressure paths, one for punch No. 1 and the other for the punch No. 2. Investigating of value and quality of the tube formability was carried out in various pressure paths based on the full factorial DOE which resulted in 16 (=4\*4) different pressure paths. Finally, the best mode for tube forming was selected based on thickness distribution and complete filling of mold in the BZ and TZ. Various modes are presented in

Table 5.

Table 5. various modes of axial feeding due to investigation of stainless steel tube forming in various series of the pressure path.

Simulation run No.	1	2	3	4	5	6	7	8	9	10	11	12	13	14	15	16
LAF (mm)	4	4	4	4	6	6	6	6	8	8	8	8	10	10	10	10
RAF (mm)	10	13	16	19	10	13	16	19	10	13	16	19	10	13	16	19

#### 4.1.1 Investigation of various pressure paths

As previously mentioned, three P2 were used to form the steel tube, where the pressure 36, 40 and 45 MPa, called the first, second and third series, respectively. Figure 9 shows the pressure path for the LAF and RAF in the first series. According to Table 4, the model should be run in 16 different modes and results can be seen in the appendix.

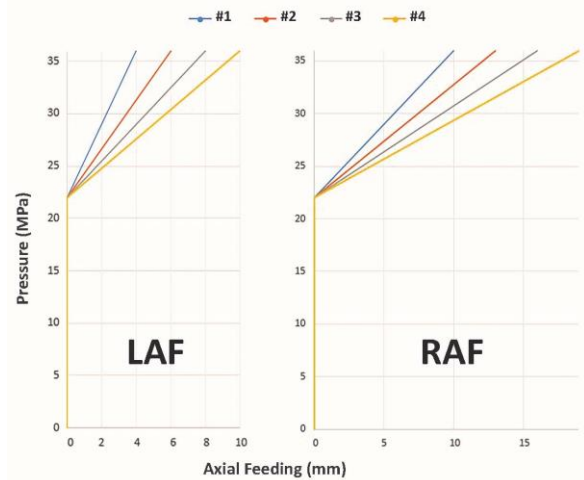


Figure 9. Left and right axial feeding in first series of the pressure path with maximum pressure of 36 MPa.

The results of the runs were shown that in almost all cases, there was wrinkling in BZ and TZ was not well filled. Among all modes, in lower-feed samples (e.g. samples #1 and #5), the BZ was formed better and less wrinkling was observed. It was also observed that with increasing the RAF (e.g. samples #4 and #8), the depth of the T was increased but severe wrinkling was observed in the BZ. Finally, in any case of the first series of pressure paths, the tube was not completely formed.

Investigations in the second series were also performed like the first series, except that in this series; the P2 was 40 MPa. In Figure 10, four pressure paths of the LAF and RAF are shown, where the possible scenarios of these paths will be 16 modes, and these runs also can be seen in the appendix.

In the first series, the axial feeding/increasing pressure ratio was higher than the other two, and this was the reason for the occurrence of wrinkling in all modes. However, in the second series, for example, in scenarios 1 and 4, this ratio was less and hence, not only any wrinkling was observed, but the mold was also relatively filled. The negative point in this series was the lack of complete filling of the corners and the existence of a gap between the tube and the mold wall. This situation can be seen in #5, #6, #9 and #13.

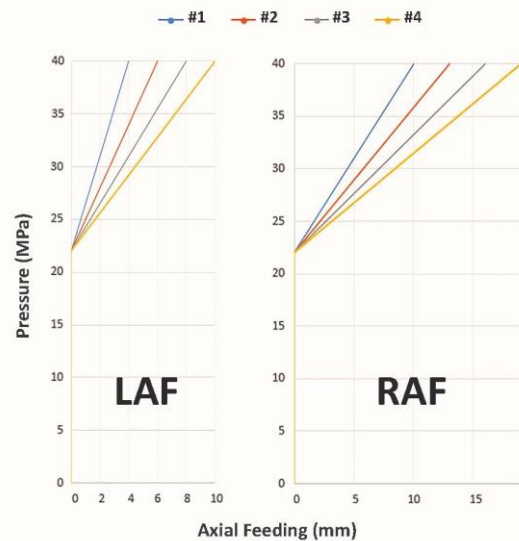


Figure 10. Left and right axial feeding in the second series of the pressure path with calibration pressure of 22.5 Mpa and maximum pressure of 40 MPa.

In order to improve the filling of the mold corners, it seemed that increasing the axial feeding will improve the situation, but, with increasing axial feeding, the wrinkles appeared in the samples. This state can be seen in #8, #11, #12, #14, #15 and #16 of the second series. In modes #7 and #10, the tube filled the mold properly, and there was no wrinkling (although corners were not completely filled in these cases). The evaluation of axial feeding in these modes was shown that the total displacement of the LAF and RAF was approximately equal (22 for #7 and 21 for #10) and the ratio of the LAF to the RAF was appropriate. The depth of the TZ in the #7 was greater than #10, but non-complete filling of the corners, as shown in Figure , led to the investigation of the third series of pressure paths.

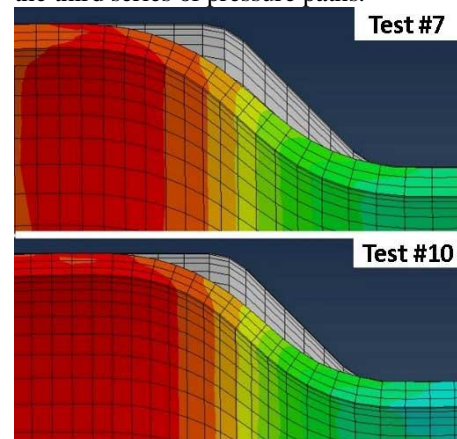


Figure 11. simulation results of non-complete filling of tests #7 and #10 tests in the second series of the pressure path.

The criteria for choosing the proper forming conditions were the complete filling of the mold, the lack of defects such as wrinkling and tearing, the greater height of the T and the appropriate thickness distribution, and since none of the modes in two previous series had satisfied all of these, the third series with the maximum pressure of 45 MPa was investigated. In Figure 11, the right and left pressure paths in the third series are observed. Like the two previous ones, in this series, the model was run in 16 different modes, and the results are shown in the appendix.

The simulation results of this series were shown that there was no effect of wrinkling in any of the modes, and the filling of the BZ was better and more than the previous two series. In some modes of this series, such as #1, #2, #5, #6 and #9, there was a gap between the tube and the mold, which two of them are shown in Figure 12.

Unlike the mentioned cases, in the #11, #12, #14, #15 and #16, the corners of the mold were completely formed, but due to the large axial feeding, a gap between the tube and the BZ wall was observed (Figure 13).

Figure 14 shows the four corners of the mold in the BZ for the remaining modes (#3, #4, #7, #8, #10 and #13). The careful examination of these images showed that except for the #3 and #4, which were less filled, the others (#7, #8, #10 and #13) were acceptable and almost similar in terms of filling and behavior.

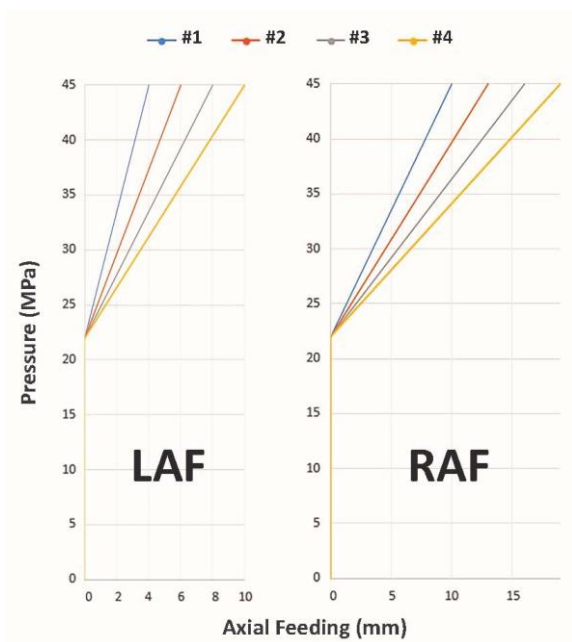


Figure 11. Left and right axial feeding in third series of the pressure path with maximum pressure of 45 MPa.

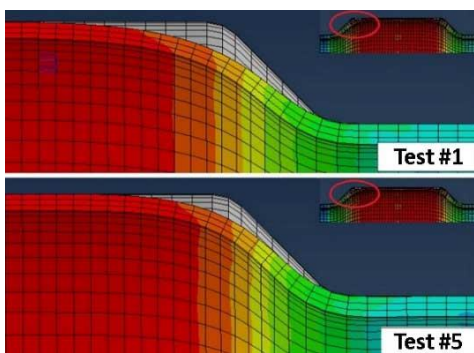


Figure 12. view of non-complete corner filling due to low axial feeding in #1 and #5 simulation runs.

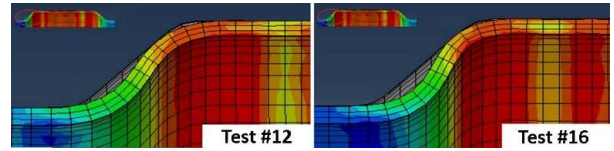


Figure 13. view of non-complete corner filling due to low axial feeding in #1 and #5 simulation runs.

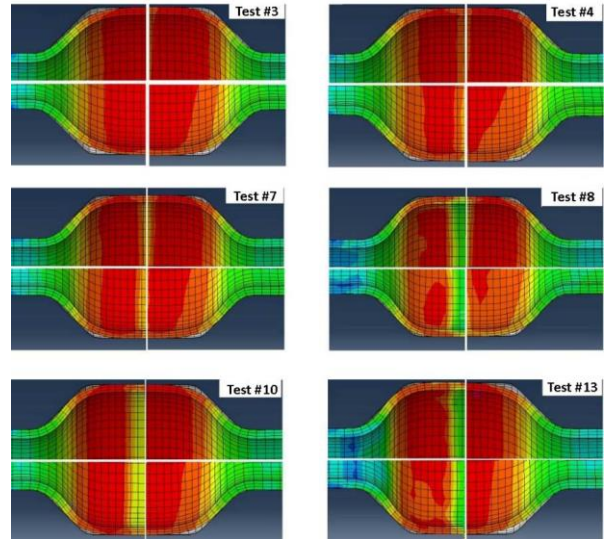


Figure 14. view of corner filling value in #3, #4, #7, #8, #10 and #13 simulation runs.

#### 4.2 T depth

In the T-shaped tube hydroforming the depth of the branch can be more by increasing the axial feeding and creating a proper material flow, but, in the specific geometry of this study; the axial feeding from the BZ side was limited and, hence, it was impossible to achieve the high depth of the TZ. In addition, with increasing axial feeding, wrinkling appear in some other areas (Figure 15). Forasmuch as the depth of the TZ was limited, the counter punch was considered fixed in the simulation and the forming process.

Considering the simulated images of the four selected samples, as can be seen in the appendix, was shown that #8, with a 6 mm LAF and an RAF of 19 mm, has the highest depth of TZ.

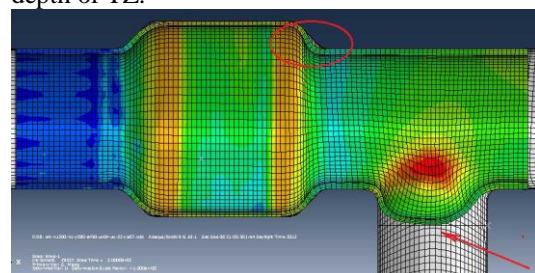


Figure 15. a sample of high right axial feeding and its tee depth and corner filling.

#### 4.3 BZ thickness distribution

Examination of the samples in terms of the distribution of the thickness in the BZ was the final step for selecting the best sample. The thickness distribution was extracted on the two sides of the BZ, one on the TZ side, and the other on the opposite side (as shown in Figure 16), and were brought.

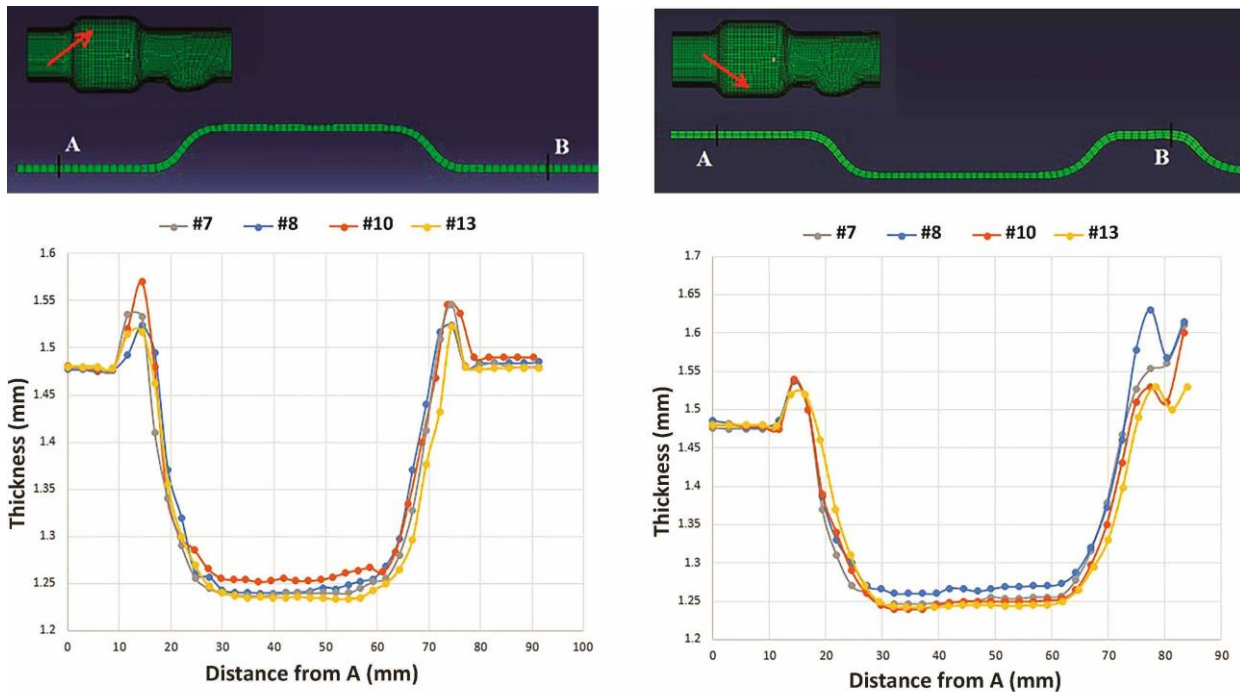


Figure 16. thickness distribution diagram of tests #7, #8, #10 and #13.

Performing a free bulge test on several tubes determined the approximate thickness of the tube wall after tearing, which was about 0.9 mm (Figure 17), and according to the diagrams of thickness distribution of Figure 16, it was found that no samples will not reach to tear. Therefore, it was found that sample #8 had the least degree of thinning and the best thickness distribution.



Figure 17. tearing in weld seams in stainless steel tubes.

Finally, based on the profile of the formed tube, the depth of the T and the BZ thickness distribution, it was found that the sample #8, in the third series of pressure paths with the maximum pressure of 45 MPa, LAF of 6 mm and a 19 mm RAF, was the best choice for forming a SS304 tube with The thickness of 1.5 mm.

#### 4.4 70/30 brass tubes

The procedure of finding the best forming condition was done for brass similar to the steel tubes. In this regard, the investigation of different pressure paths was carried out for the LAF values of 2, 4, 6 and 8 mm and the RAF of 4, 8, 12 and 16 mm and at two maximum pressure levels of 12.5 MPa and 14.5 MPa. Lower values of maximum pressure in the brass tubes forming correspond to its lower yield strength and thickness. Finally, based on the full factorial DOE, 16 different forming modes were investigated at each pressure level (totally  $32 = 2 * 4 * 4$ -

Table 6).

Table 6. various modes of axial feeding due to investigation of stainless steel tube forming in various series of the pressure path.

Simulation run No.	1	2	3	4	5	6	7	8	9	10	11	12	13	14	15	16
LAF (mm)	2	2	2	2	4	4	4	4	6	6	6	6	8	8	8	8
RAF (mm)	4	8	12	16	4	8	12	16	4	8	12	16	4	8	12	16

The pressure path diagrams for the first pressure level are shown in Figure 18 and as is clear, in all paths, the pressure was increased up to 10 MPa, until the calibration was performed, and then the axial feeding and pressure were increased simultaneously, in different paths. Diagrams of the

second level were exactly like the mentioned case with only a maximum pressure of 14.5 MPa. Images of different simulation modes for these two levels of pressure are shown in the appendix.

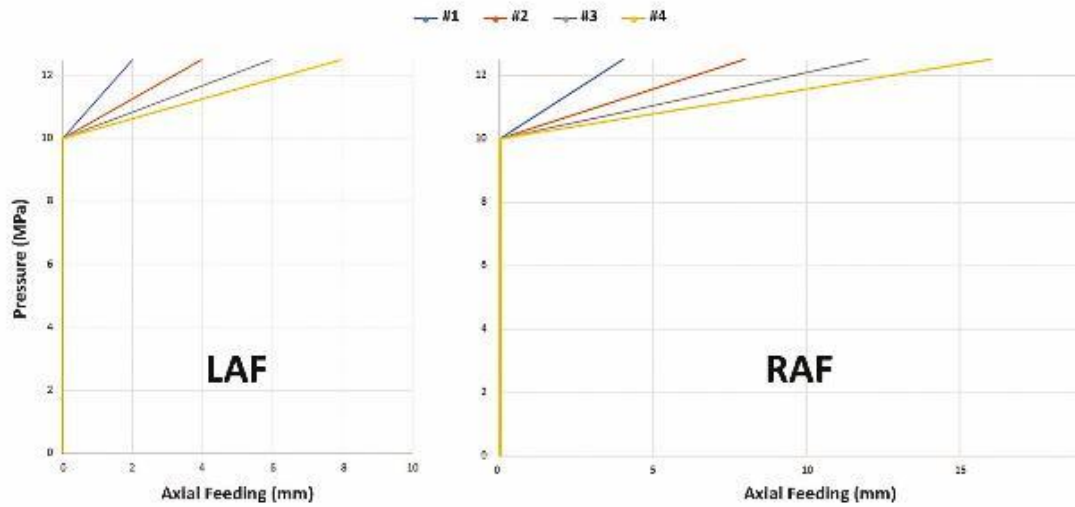


Figure 18. Left and right axial feeding in first series of the pressure path with maximum pressure of 12.5 MPa.

The results of various modes of the model run at the first level of pressure were shown that the maximum pressure of 12.5 MPa is low for the execution of the forming process. The reason for this allegation is that in cases where the axial feeding was high, for example, RAF of 12 mm or more, wrinkling was observed, and in other cases where no wrinkles occurred, the tube did not completely fill the mold. Therefore, none of the modes of this level were provided a satisfactory result for the formation of brass tubes. The simulation results of the second level modes were shown that in almost all cases, the filling level of the BZ was higher than the first level. Among the reviewed cases, it was found

that in #4, #7, #10 and #11, the BZ was formed without any wrinkling, and views of their corners are shown in Figure 19 for a closer look.

Investigation of Figure 19 was shown that in #4 and #7, the formation of the BZ was good and the corners were formed well, but in the #10, the corners were not filled well and in #11, due to the large RAF, a slight gap was observed between tube and mold, which was indicating that the tube was exposed to wrinkling. The selection of the final choice from the #4 and #7 scenarios were done based on the TZ filling and BZ thickness distribution.

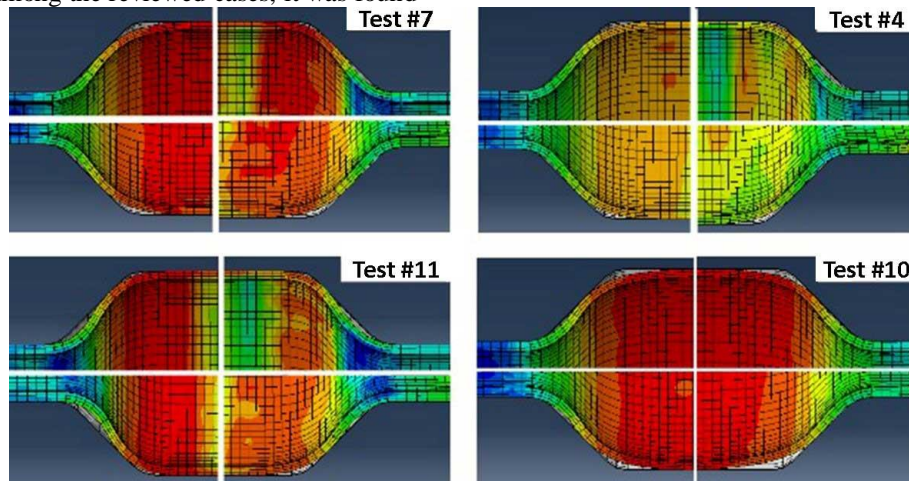


Figure 19. view of corner filling value in #4, #7, #10 and #11 simulation runs.

#### 4.5 T depth

Comparison of filling rate in TZ between the two remaining samples was carried out using the displacement contour (U) results, which are shown in Figure 20, and it was found that the filling rate in #4 was greater than the #7. Based on the similarity of the pressure variations in two modes, and the 4 mm greater axial feeding of #4 than #7 (16 versus 12), the results were foreseeable. As noted earlier, with more

increasing of the axial feeding, despite increasing the depth of the T, the wrinkling will appear in the tube.

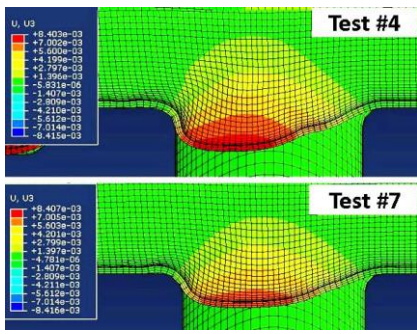


Figure 20. determination of tee zone filling using the displacement contour.

#### 4.5.1 BZ Thickness distribution

The distribution of the thickness in the BZ on the two sides of the tube is shown in Figure 21 for simulated samples and after running of the model.

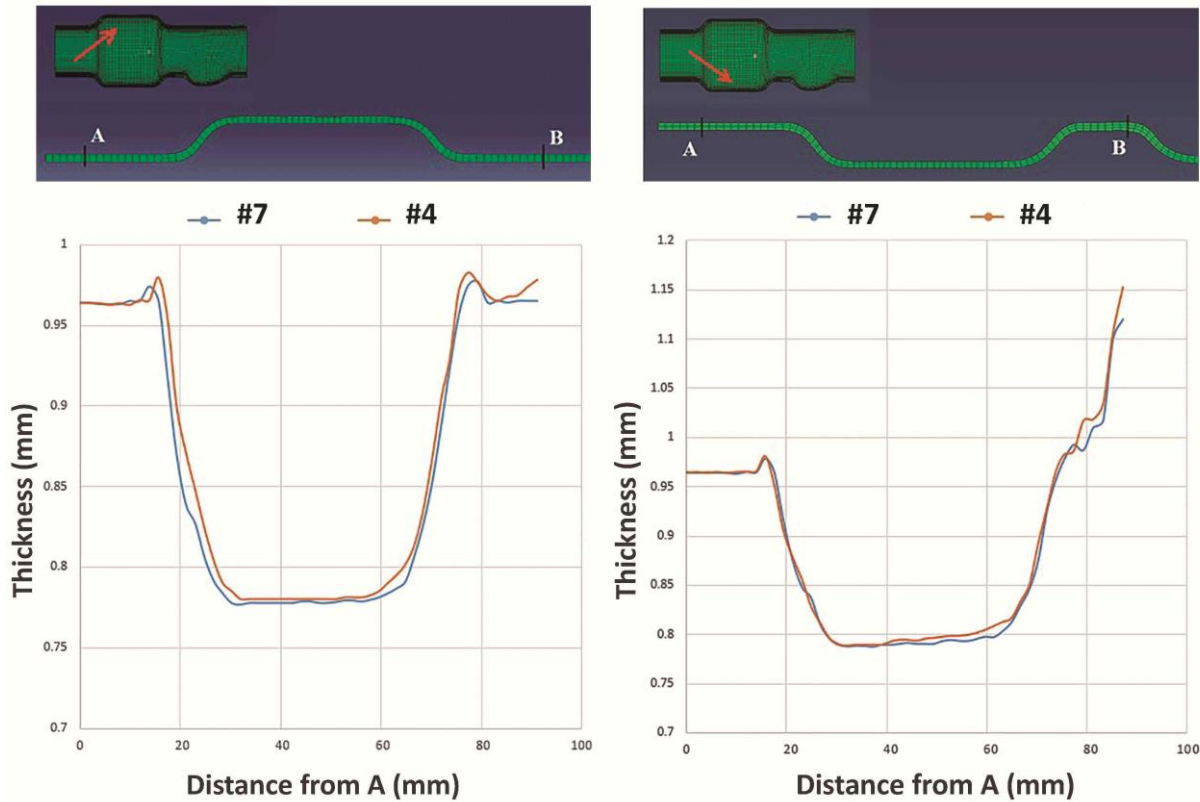


Figure 21. thickness distribution diagram of tests No. #4 and #7.

Based on free bulge tests, which an example is shown in Figure 22, it was found that the thickness of the brass tube at the time of tearing is approximately 0.73 mm, so tearing will not occur in any of the samples. The graphs were shown that the thickness of the two samples was almost the identical, but the thickness of #4 was a little more.

Comparison of the thickness between the upper and lower parts of the BZ showed that the thickness of the part located near the TZ was higher than the other part. This phenomenon was occurred due to more demand for material flow from the T-side, which this flow contributed to less thinning of the tube, but in the upper part, as this demand did not exist, the tube was thinned for complete forming.



Figure 22. bulge test undertaken on the 70/30 brass tube and tearing occurred in thickness about 0.73mm.

#### 4.6 Choosing best pressure path and healthy produce final piece

The conclusions of the above items were shown that mode #4 provided optimal pressure path and forming conditions for a 1 mm thick 70/30 brass tube; these conditions were included a maximum pressure of 14.5 MPa, an RAF of 16 mm, and an LAF of 2 mm, and by them, the desired profile

was formed with appropriate thickness distribution and complete mold filling.

In the specific geometry of this study, increasing the height and improvement the filling of the TZ, were possible with increasing the axial feeding or pressure. However, due to the limitation in LAF (possibility of wrinkling), increasing the pressure, after it reaches to the maximum, was the only way, which an example of this for brass tube is shown in Figure 23, and the simulated model and formed tube can be seen in Figure 24.

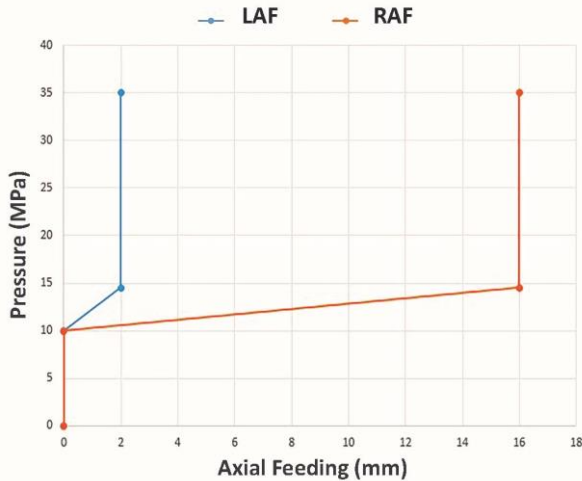


Figure 23. final pressure path in order to complete forming the 70/30 brass tube.

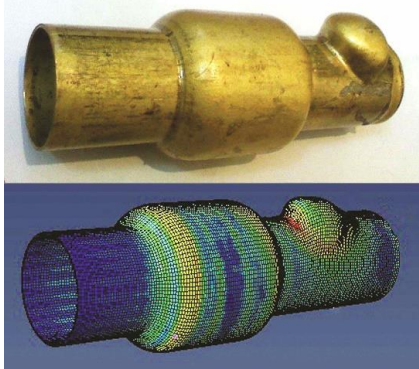


Figure 24. experimental and simulation results of the formed tube with the final chosen pressure path.

## 5. Conclusion

In the present study, the formation of some special or combined geometries on stainless steel and brass tubes were investigated by both simulation and experiments. To be specific, finite element (FE) model was used to achieve the best forming conditions for 304 stainless steel and 70/30 brass tubes. Then, for various combinations of axial feeding and pressure variations, based on the full factorial DoE, the model was run and the preferred forming mode was selected based on the better filling of the mold and the more appropriate thickness distribution.

The asymmetry of the studied geometry was limited the material flow from the middle of the tube towards the T-zone, and hence the height of T was limited. During the forming operation, with increasing the deformation and

thinning, stresses were concentrated on the weld seam, and tearing occurred from that region.

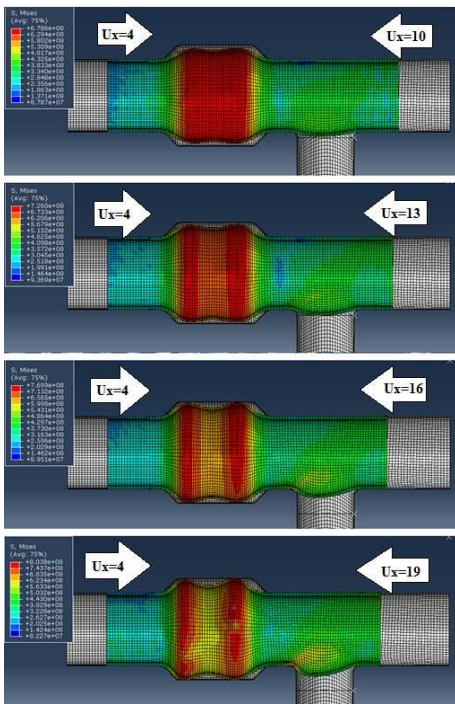
The results of various simulations were shown that for the steel tubes, the calibration pressure of 22.5 MPa, the maximum pressure of 45 MPa, the right and left axial feeding of 19 mm and 6 mm were appropriate, while the same values for the brass tube were 10 MPa, 14.5 MPa, 16 mm and 2 mm, respectively. Finally, a sample was formed according to optimal conditions obtained from the simulation process.

## 6. Reference

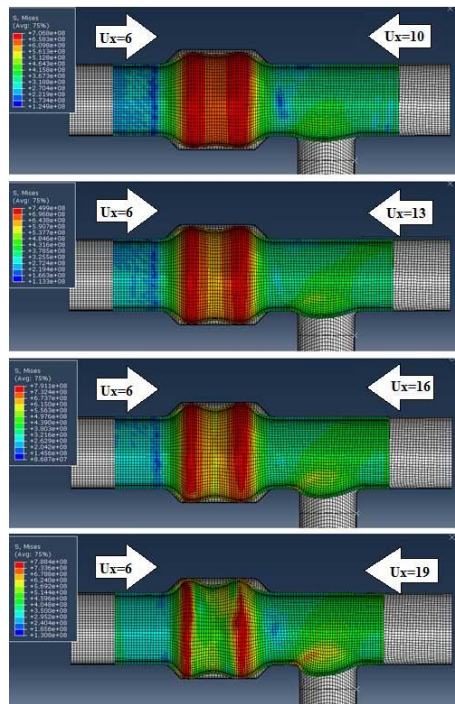
- [1] P. Thanakijkasem, A. Pattarangkun, S. Mahabunphachai, V. Uthaisangasuk, S. Chutima, Comparative study of finite element analysis in tube hydroforming of stainless steel 304, *International Journal of Automotive Technology*, Vol. 16, No. 4, pp. 611-617, August 01, 2015.
- [2] N. Abedrabbo, M. A. Zampaloni, F. Pourboghraat, Wrinkling control in aluminum sheet hydroforming, *International Journal of Mechanical Sciences*, Vol. 47, No. 3, pp. 333-358, 2005/03/01/, 2005.
- [3] L. H. Lang, Z. R. Wang, D. C. Kang, S. J. Yuan, S. H. Zhang, J. Danckert, K. B. Nielsen, Hydroforming highlights: sheet hydroforming and tube hydroforming, *Journal of Materials Processing Technology*, Vol. 151, No. 1, pp. 165-177, 2004/09/01/, 2004.
- [4] T. Intarakumthornchai, Y. Aue-U-Lan, R. Kesvarakul, S. Jirathearanat, Feasible pressure and axial feed path determination for fuel filler tube hydroforming by genetic algorithm, *Proceedings of the Institution of Mechanical Engineers, Part B: Journal of Engineering Manufacture*, Vol. 229, No. 4, pp. 623-630, 2015.
- [5] W. Zhuang, S. Wang, J. Cao, J. Lin, C. Hartl, Modelling of localised thinning features in the hydroforming of micro-tubes using the crystal-plasticity FE method, *The International Journal of Advanced Manufacturing Technology*, Vol. 47, No. 9, pp. 859-865, April 01, 2010.
- [6] A. Alaswad, K. Y. Benyounis, A. G. Olabi, Tube hydroforming process: A reference guide, *Materials & Design*, Vol. 33, pp. 328-339, 2012/01/01/, 2012.
- [7] G. N. Chu, G. Liu, W. J. Liu, S. J. Yuan, An approach to improve thickness uniformity within tailor-welded tube hydroforming, *The International Journal of Advanced Manufacturing Technology*, Vol. 60, No. 9, pp. 1247-1253, June 01, 2012.
- [8] R. Hashemi, M. B. Shirin, M. Einolghozati, A. Assempour, A different approach to estimate the process parameters in tube hydroforming, *International Journal of Material Forming*, Vol. 8, No. 3, pp. 355-366, July 01, 2015.
- [9] C. Han, H. Feng, L. D. Yan, S. J. Yuan, Thickness improvement in non-homogeneous tube hydroforming of a rectangular component by contact sequence, *The International Journal of Advanced Manufacturing Technology*, Vol. 92, No. 5, pp. 2667-2675, September 01, 2017.
- [10] N. Abedrabbo, N. Zafar, R. Averill, F. Pourboghraat, R. Sidhu, 2004, *Optimization of a Tube Hydroforming Process*,
- [11] B. Teng, K. Li, S. Yuan, Optimization of loading path in hydroforming T-shape using fuzzy control algorithm, *The International Journal of Advanced Manufacturing Technology*, Vol. 69, No. 5, pp. 1079-1086, November 01, 2013.

- [12] Y.-l. Ge, X.-x. Li, L.-h. Lang, S.-w. Ruan, Optimized design of tube hydroforming loading path using multi-objective differential evolution, *The International Journal of Advanced Manufacturing Technology*, Vol. 88, No. 1, pp. 837-846, January 01, 2017.
- [13] A. Ben Abdesslem, A. El-Hami, Global sensitivity analysis and multi-objective optimisation of loading path in tube hydroforming process based on metamodeling techniques, *The International Journal of Advanced Manufacturing Technology*, Vol. 71, No. 5, pp. 753-773, March 01, 2014.
- [14] A. Abdelkefi, P. Malécot, N. Boudeau, N. Guermazi, N. Haddar, On the tube hydroforming process using rectangular, trapezoidal, and trapezoid-sectional dies: modeling and experiments, *The International Journal of Advanced Manufacturing Technology*, Vol. 93, No. 5, pp. 1725-1735, November 01, 2017.
- [15] R. Di Lorenzo, G. Ingarao, F. Chinesta, Integration of gradient based and response surface methods to develop a cascade optimisation strategy for Y-shaped tube hydroforming process design, *Advances in Engineering Software*, Vol. 41, No. 2, pp. 336-348, 2010/02/01/, 2010.
- [16] Z. Yu, Q. Kong, C. Ma, Z. Lin, Theoretical and experimental study on formability of laser seamed tube hydroforming, *The International Journal of Advanced Manufacturing Technology*, Vol. 75, No. 1, pp. 305-315, October 01, 2014.
- [17] G. Faraji, R. Hashemi, M. M. Mashhadi, A. F. Dizaji, V. Norouzfard, Hydroforming Limits in Metal Bellows Forming Process, *Materials and Manufacturing Processes*, Vol. 25, No. 12, pp. 1413-1417, 2010/12/03, 2010.
- [18] L. Yang, G. Hu, J. Liu, Investigation of forming limit diagram for tube hydroforming considering effect of changing strain path, *The International Journal of Advanced Manufacturing Technology*, Vol. 79, No. 5, pp. 793-803, July 01, 2015.
- [19] Y. P. Korkolis, S. Kyriakides, Hydroforming of anisotropic aluminum tubes: Part II analysis, *International Journal of Mechanical Sciences*, Vol. 53, No. 2, pp. 83-90, 2011/02/01/, 2011.
- [20] Korkolis, S. Kyriakides, Hydroforming of anisotropic aluminum tubes: Part I experiments, *International Journal of Mechanical Sciences*, Vol. 53, No. 2, pp. 75-82, 2011/02/01/, 2011.
- [21] M. Mirzaali, S. M. H. Seyedkashi, G. H. Liaghat, H. Moslemi Naeini, K. Shojaei G, Y. H. Moon, Application of simulated annealing method to pressure and force loading optimization in tube hydroforming process, *International Journal of Mechanical Sciences*, Vol. 55, No. 1, pp. 78-84, 2012/02/01/, 2012.
- [22] W. Zhuang, S. Wang, J. Lin, D. Balint, C. Hartl, Experimental and numerical investigation of localized thinning in hydroforming of micro-tubes, *European Journal of Mechanics - A/Solids*, Vol. 31, No. 1, pp. 67-76, 2012/01/01/, 2012.
- [23] M. Koç, Y. Aue-u-lan, T. Altan, On the characteristics of tubular materials for hydroforming—experimentation and analysis, *International Journal of Machine Tools and Manufacture*, Vol. 41, No. 5, pp. 761-772, 2001/04/01/, 2001.
- [24] M. G. Stout, K. P. Staudhammer, Biaxial deformation of 70-30 brass: Flow behaviors, texture, microstructures, *Metallurgical and Materials Transactions A*, Vol. 15, No. 8, pp. 1607, August 01, 1984.

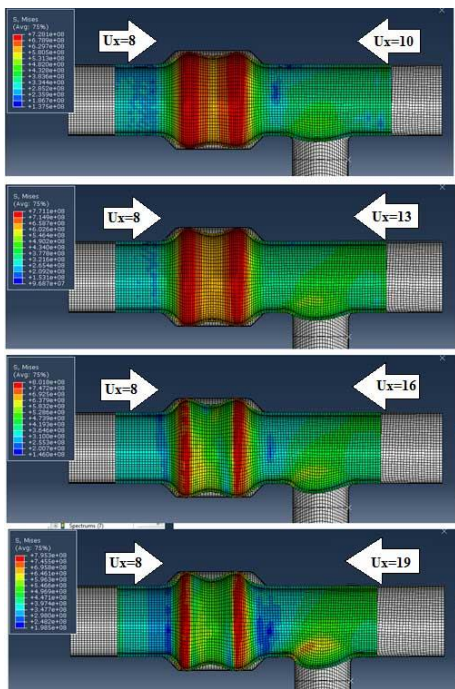
7. APPENDIX



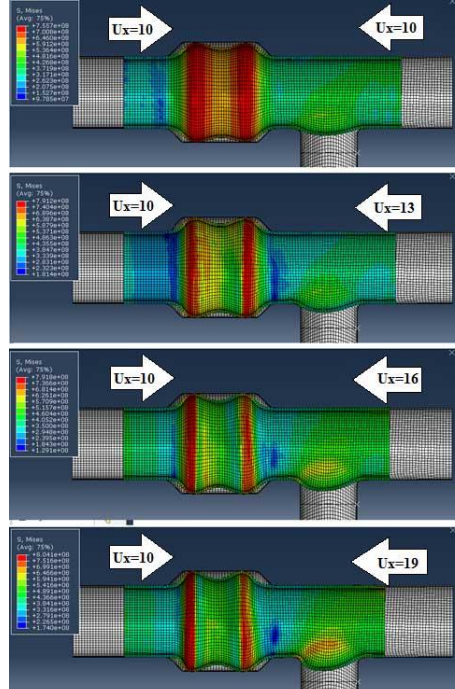
SS304 tube- first series of pressure path (No. #1 to #4 of table 5)



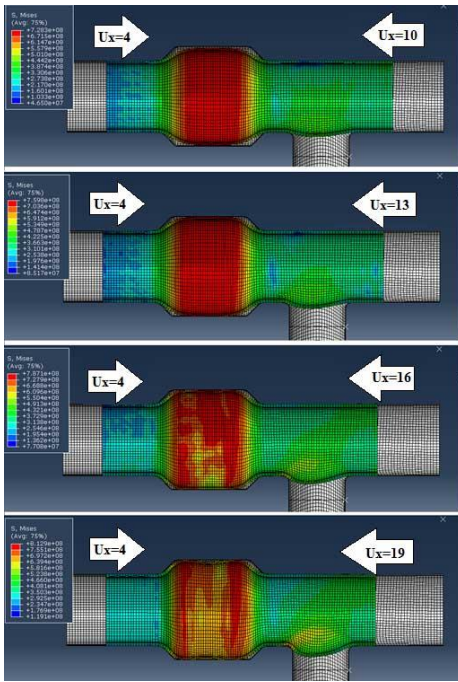
SS304 tube- first series of pressure path (No. #5 to #8 of table 5)



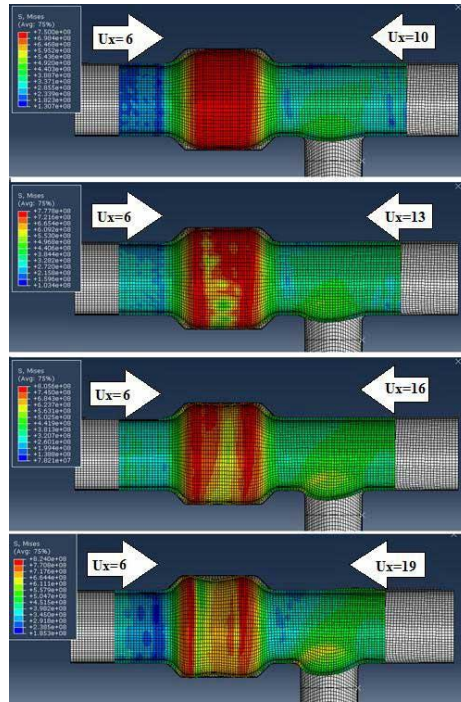
SS304 tube- first series of pressure path (No. #9 to #12 of table 5)



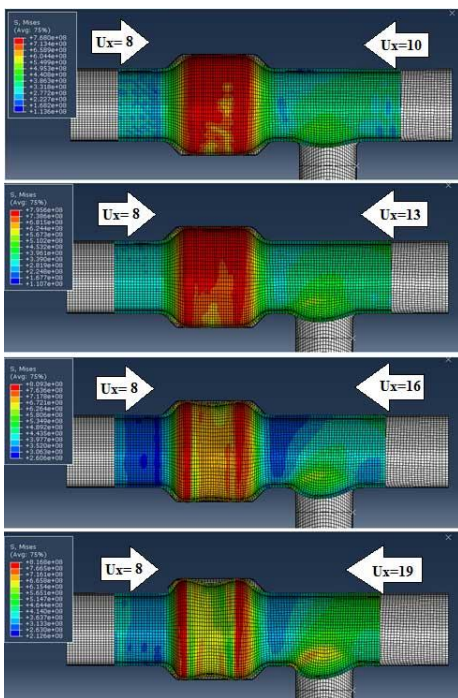
SS304 tube- first series of pressure path (No. #13 to #16 of table 5)



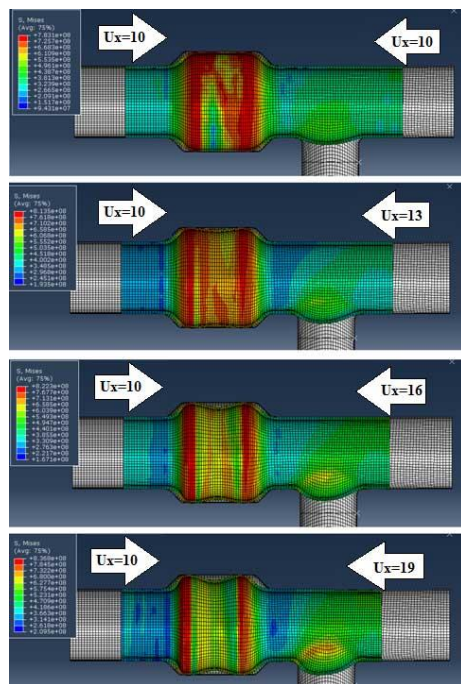
SS304 tube- second series of pressure path (No. #1 to #4 of table 5)



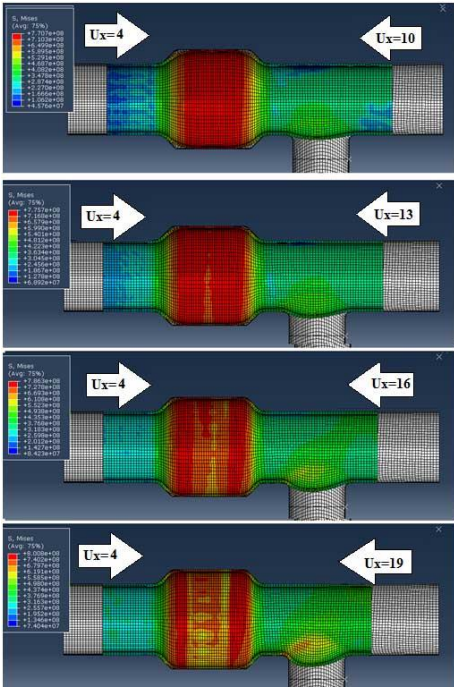
SS304 tube- second series of pressure path (No. #5 to #8 of table 5)



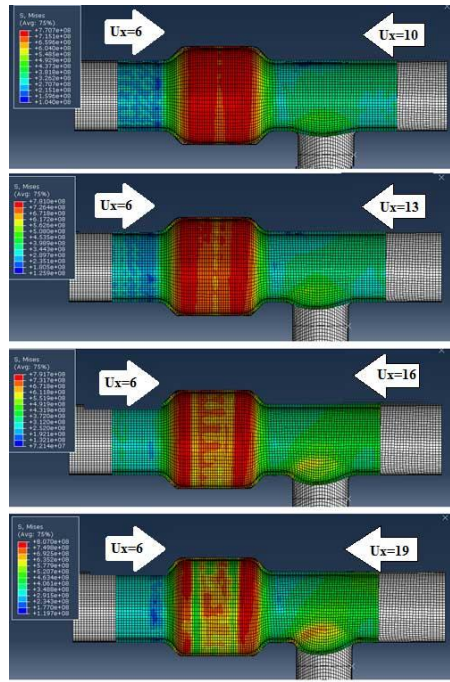
SS304 tube- second series of pressure path (No. #9 to #12 of table 5)



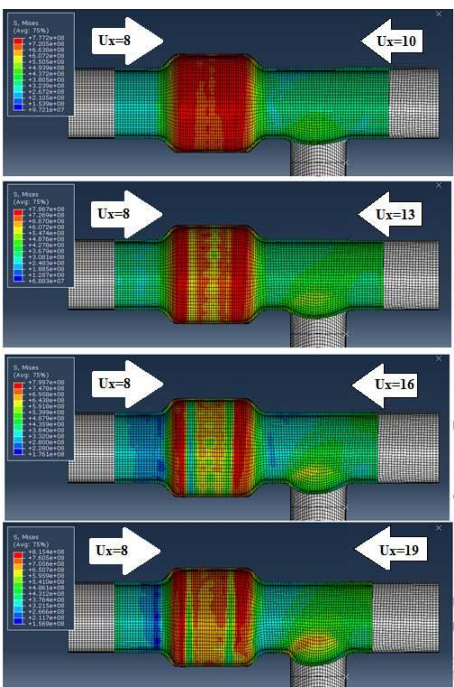
SS304 tube- second series of pressure path (No. #13 to #16 of table 5)



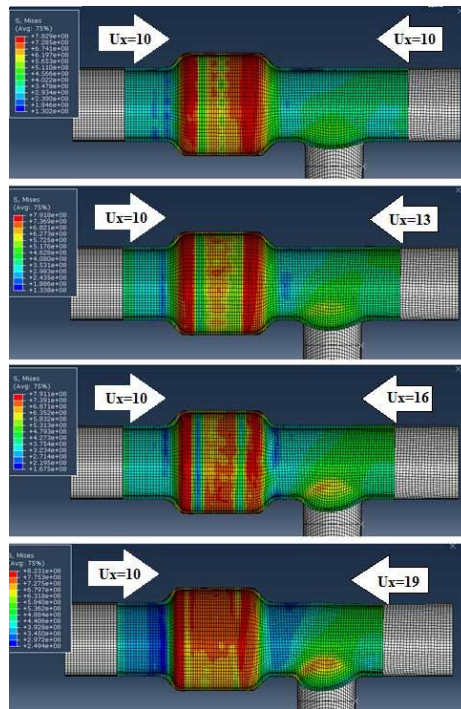
SS304 tube- third series of pressure path (No. #1 to #4 of table 5)



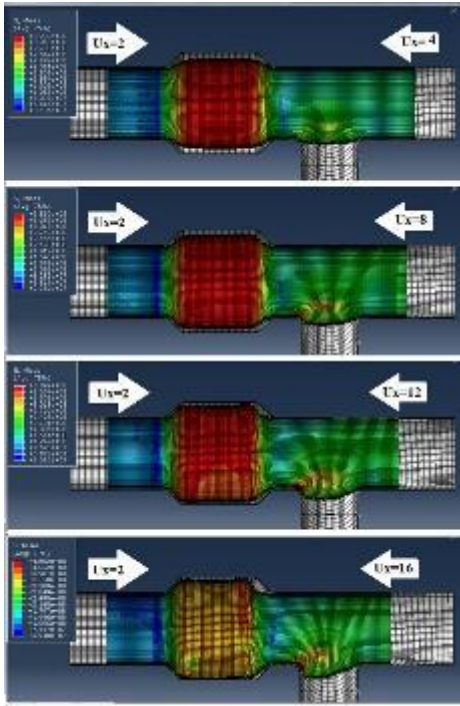
SS304 tube- third series of pressure path (No. #5 to #8 of table 5)



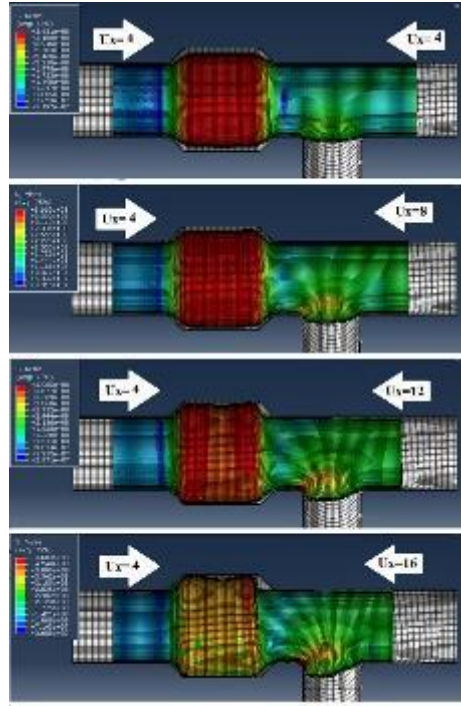
SS304 tube- third series of pressure path (No. #9 to #12 of table 5)



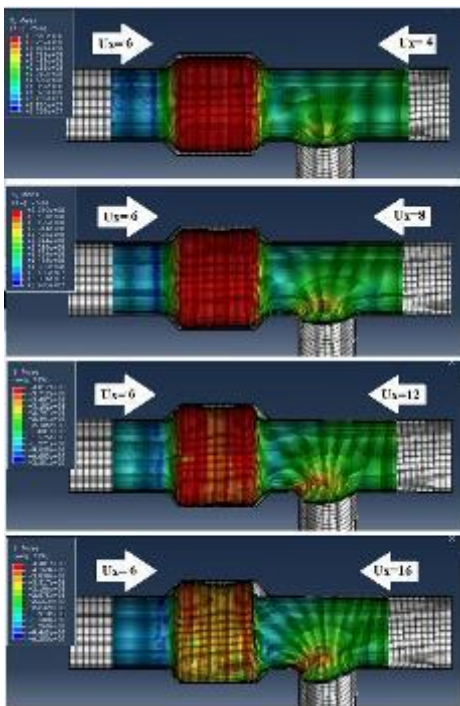
SS304 tube- third series of pressure path (No. #13 to #16 of table 5)



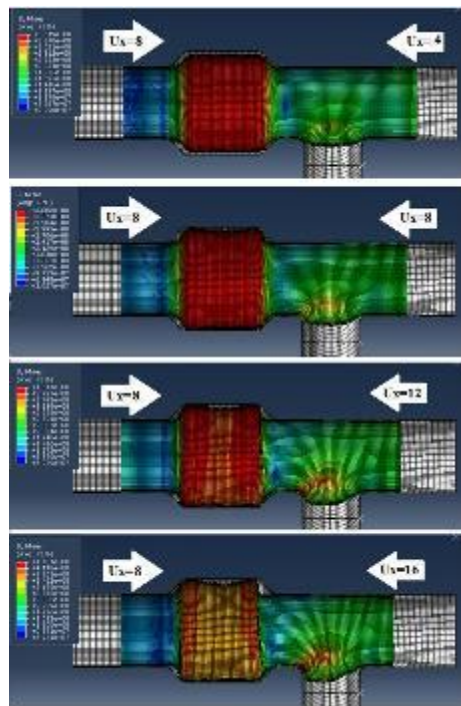
Brass tube- first series of pressure path (No. #1 to #4 of table 6)



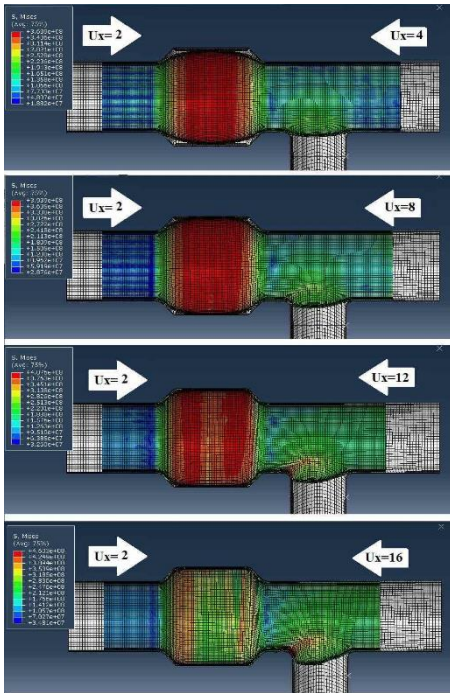
Brass tube- first series of pressure path (No. #5 to #8 of table 6)



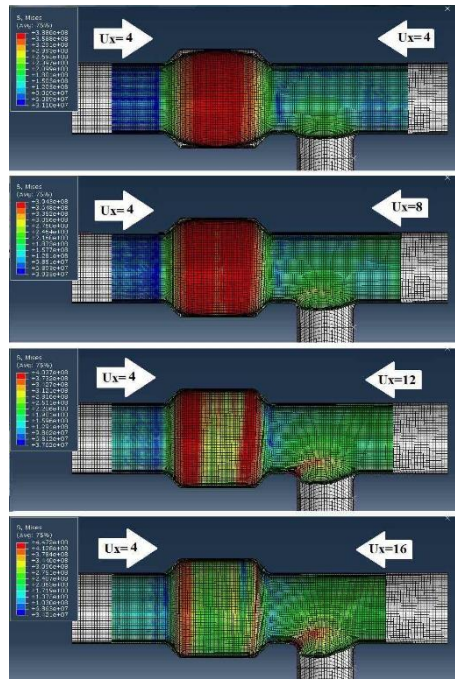
Brass tube- first series of pressure path (No. #9 to #12 of table 6)



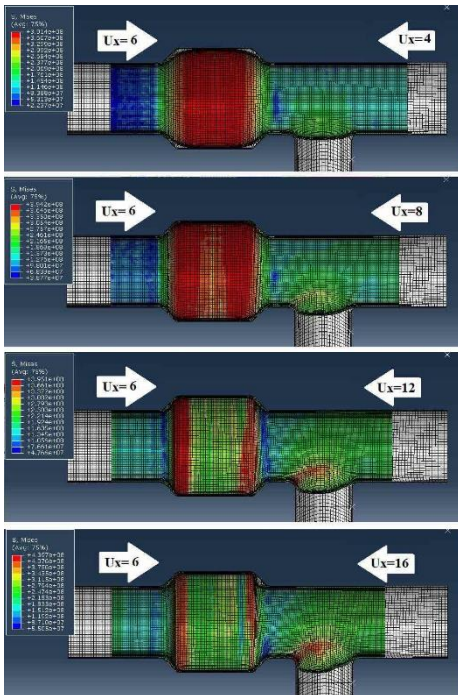
Brass tube- first series of pressure path (No. #13 to #16 of table 6)



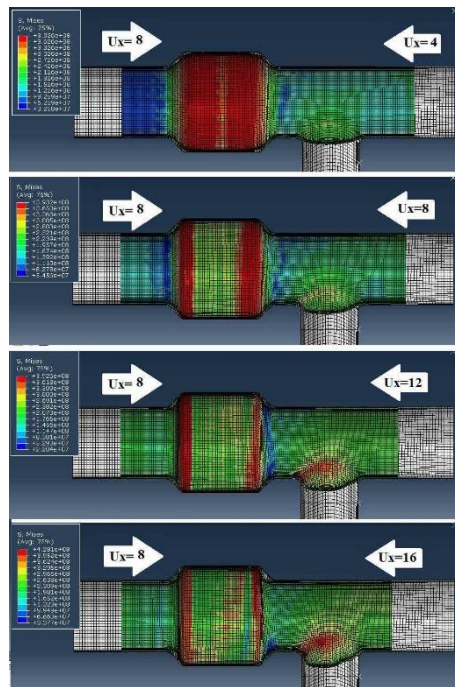
Brass tube- second series of pressure path (No. #1 to #4 of table 6)



Brass tube- second series of pressure path (No. #5 to #8 of table 6)



Brass tube- second series of pressure path (No. #9 to #12 of table 6)



Brass tube- second series of pressure path (No. #13 to #16 of table 6)